# DEVELOPMENT OF A SOFTWARE ARCHITECTURE FOR COMPARING EXISTING ORBITAL CARRYING CAPACITY MODELS

**Lorenzo Giudici (1), Mario Neri (1)**

(1) *Telesat, 160 Elgin St Suite, ON K2P 2P7 Ottawa, Canada, Email: lgiudici@telesat.com mneri@telesat.com*

## ABSTRACT

This paper addresses the concept of “Orbital Carrying Capacity” (OCC), in light of the increasing reliance of today’s activities on space technologies and consequent recent growth of the satellites’ population. Although there is no internationally agreed-upon definition, OCC generally refers to the maximum sustainable use of orbital resources, safeguarding their availability for future generations. Rather than elaborating a new, competing definition of OCC, this paper focuses on comparing a number of existing models already available in literature to measure OCC, with the aim to offer clear insights into their effectiveness when evaluated across different scenarios of future space activity. To ensure a robust comparison, a consistent underlying objects population model is used across all analyses, guaranteeing that any differences in results stem solely from the way OCC is measured in each of the studied models. The ultimate goal is to offer further means for making informed decisions when selecting appropriate models for measuring orbital resource consumption, considering the different nature and characteristics of the space systems involved.

## 1 INTRODUCTION

The recent rapid increase in human dependence on space activities and the resulting growth of satellite population have led the space community to question the residual availability of space resources and to attempt defining the concept of “Orbital Carrying Capacity (OCC).” Currently, there is no internationally-agreed definition of OCC, although it can be stated that, in general, the concept refers to the maximum physical occupancy available for space missions that, given the way space assets are designed, deployed, operated and disposed of, ensures a long-term sustainable evolution of the orbital environment, so that future generations can continue to access it. While there is general agreement on the meaning of OCC, how to measure it is widely debated, given the complexity of the problem at hand.

Several attempts have been made to define metrics and associated thresholds for OCC. In some cases, these efforts have even led to proposals for methodologies to manage residual orbital resources [1]. From the authors' perspective, there are two main approaches to measuring OCC in literature. The first, referred to as the “object-based” approach in this paper, quantifies the OCC as the maximum number of satellites that can be deployed in orbit in a sustainable way within altitude shells defined arbitrarily. The second approach, referred to as “risk-based,” correlates the residual availability of orbital resources with the cumulative risk to the orbital environment posed by the current and projected populations of spacecraft. This latter approach further branches into several formulations, each considering a different definition of risk [2].

In this context, Telesat, similar to other stakeholders [3][4][5], believes that there is the need to carry out technical studies to provide a more comprehensive understanding of existing models for quantifying OCC, rather than define yet a new model that would risk to add further divergence in literature. Therefore, the primary objective of this paper is to provide additional insights on how the different OCC models compare, with the ultimate goal of providing means to interpret the results these models provide and of ensuring greater awareness on the topic. This would enable the possible use of the concept of orbital carrying capacity within a regulatory context, should this be ever needed, in a manner that is responsible and based on scientific evidence.

The paper is organized as follows: Section 2 introduces the objects’ population model adopted in this study to support the analysis of the OCC modelling approaches. Section 3 presents the investigated OCC formulations from a theoretical viewpoint. Section 4 provides the results of their application and compares the various formulations under different scenarios. Finally, Section 5 summarizes the key findings of this work based on the authors' interpretation of the relevant results.

## 2 OBJECTS POPULATION MODEL

This section provides a concise overview of the objects’ population model used for the analyses of OCC presented in this paper. The approach used to characterise the in-orbit spacecraft population belongs to the category of source-sink debris evolutionary models, often referred to as Particle-In-a-Box (PIB) models, which encompass various formulations that have been developed over the years and can be found in literature. Examples are the PODEM [6], STAT [7], MISSD [8] and MOCAT [9] models. In this work, the formulation proposed by Sturza

*Proc. 9th European Conference on Space Debris, Bonn, Germany, 1–4 April 2025, published by the ESA Space Debris Office*
*Editors: S. Lemmens, T. Flohrer & F. Schmitz, (http://conference.sdo.esoc.esa.int, April 2025)*

et al. (2022) [10] has been used as reference, although some modifications have been made to enhance the accuracy compared to the original model, at least from the authors' perspective.

Compared to more complex evolutionary models that account for the individual dynamics of each object [11][12], the PIB models mentioned above offer a significant advantage in terms of computational efficiency. Despite a less accurate definition of the satellites' mission profiles and a simplified representation of orbital dynamics, their efficiency makes them highly valuable for preliminary assessments.

Data on the population of objects currently in orbit is obtained from publicly available databases. In the current implementation, the software that Telesat has developed (the "Telesat software tool") and that this paper is based on automatically queries both SpaceTrack.org [13] and DISCOS [14] databases to collect information on the type, name, orbital parameters, physical characteristics, and launch/release epochs of catalogued space objects. This population is then classified into distinct categories. With respect to the approach outlined in [10], this study employs a more refined classification that distinguish some of the existing satellite constellations (e.g., Starlink and OneWeb) from the broader category of active payloads. This distinction allows to specify independently their characteristics, such as size, manoeuvrability and post-mission disposal rate, given their significant share of satellites currently in orbit. As a result, a total of nine classes are considered: active and inactive Starlink satellites, active and inactive OneWeb satellites, other active payloads, inactive payloads, rocket bodies, Lethal Trackable (LT) and Lethal Non-Trackable (LNT) debris. It is important to note that the Telesat software tool, which operates with clearly defined input files, allows for modelling as many classes as desired, although this will come at the expense of increased computational burden. Additionally, categories that do not belong to missions currently in orbit can be included to simulate the deployment of new systems, specifying a deployment rate along with all other relevant characteristics.

The Low-Earth Orbit (LEO) region is divided into a user-defined number of equally-spaced altitude shells (the analyses in Section 3 consider a shell thickness of 25 km), and every class of objects is modelled as a $N \times 1$ state vector, with elements representing the number of objects in each altitude shell. Differential equations are formulated for every objects' class, with the expression of each depending on the class' type.

For classes of active satellites, the following equation applies [10]:

$$\frac{\partial \boldsymbol{A}}{\partial t} = \frac{\boldsymbol{a} - \boldsymbol{A}}{\zeta_A} - \boldsymbol{F}_A - \boldsymbol{G}_A \tag{1}$$

where $\boldsymbol{A}$ is the state vector of one of the active satellites' classes; $\boldsymbol{a}$ is the number of satellites launched over a period of time equal to the satellite's lifetime, $\zeta_A$; $\boldsymbol{F}_A$ and $\boldsymbol{G}_A$ denote the catastrophic and non-catastrophic collision rates, respectively. The difference between these two types of collisions, as modelled in this work, is that catastrophic events result in the complete destruction of the satellite and subsequent ejection of fragments, while non-catastrophic events render a satellite unfunctional without releasing any debris. All these variables are vectors with dimension $N \times 1$, where each element represents the related quantity in one altitude shell.

For inactive satellites' classes, the corresponding differential equation reads as:

$$\frac{\partial \boldsymbol{I}}{\partial t} = \frac{(1 - \delta_A)}{\zeta_A}\boldsymbol{A} - \boldsymbol{\Phi}[\boldsymbol{d}_I \cdot \boldsymbol{I}] - \boldsymbol{F}_I + \boldsymbol{G}_A \tag{2}$$

where $\boldsymbol{I}$ is the state vector of one of the inactive satellites' class and $\boldsymbol{F}_I$ the related catastrophic collision rate vector; $\boldsymbol{A}$ refers to the active satellites' counterpart of $\boldsymbol{I}$, and $\boldsymbol{G}_A$ is its associated non-catastrophic collision rate vector; $\boldsymbol{d}_I$ is the $N \times 1$ decay rate vector to account for the orbits' contraction induced by atmospheric drag, which depends on the average area-to-mass ratio of the satellites in the $I$ class; $\delta_A$ is the post-mission disposal rate of the active satellites of the $A$ class; $\boldsymbol{\Phi}$ is a $N \times N$ matrix that models the transition of naturally decaying objects to the next lower altitude shell, which takes the form:

$$\Phi = \boldsymbol{I} - \boldsymbol{U_N} \tag{3}$$

where $\boldsymbol{I}$ and $\boldsymbol{U_N}$ are the identity and upper shift matrices, respectively.

For classes of derelict intact objects which do not have an active counterpart, like rocket bodies, the differential equation can be obtained by eliminating from Eq. (2) any term associated with the $A$ class.

Finally, for the two debris classes the following equation holds:

$$\frac{\partial \boldsymbol{D}}{\partial t} = -\boldsymbol{\Phi}[\boldsymbol{d}_D \cdot \boldsymbol{D}] - \boldsymbol{F}_D + \boldsymbol{\Theta}\boldsymbol{C}_D \tag{4}$$

The first two terms have the exact same meaning as in Eq. (2) but here refer to one of the two classes of debris. The last term describes the creation and dispersion of fragments due to catastrophic collision events from interactions between objects of every class. In particular, $\boldsymbol{C}_D$ is the $N \times 1$ debris creation rate vector, and $\boldsymbol{\Theta}$ the collision coupling matrix, which distribute the ejected fragments from collisions in one shell to all modelled shells. It is derived from fragments dispersion analyses with NASA Standard Breakup Model (SBM) [15].

Details on the equations used for evaluating every term in Eqs. (1)-(4) can be found in [10], and they are omitted here for brevity.

The state vector for each objects' class is initialized based on the orbital parameters of the objects' population currently in orbit. Since, data relative to non-trackable debris is not available in the databases by definition, the number and distribution of these small particles is initialized as a multiple of the trackable ones. According to the NASA SBM, the number of fragments ejected by a collision event of dimension $L_C$ or larger is:

$$N(L_c) = 0.1 M^{0.75} L_c^{-1.71} \tag{5}$$

with $M$ sum of the masses of the objects involved in the collision. Hence, if $d_{LNT}$ and $d_{LT}$ are the minimum diameters considered for non-trackable and trackable debris (1 cm and 10 cm, respectively, in this work), and $d_{\max}$ a reasonable maximum debris size, the non-trackable/trackable debris ratio can be obtained as:

$$\begin{aligned} \beta &= \frac{N(d_{LNT}) - N(d_{LT})}{N(d_{LT}) - N(d_{\max})} \\ &= \frac{d_{LNT}^{-1.71} - d_{LT}^{-1.71}}{d_{LT}^{-1.71} - d_{\max}^{-1.71}} \end{aligned} \tag{6}$$

If $\boldsymbol{D}_{LT}$ is the state vector for the LT debris, the state vector representing the LNT debris population is initialized to $\boldsymbol{D}_{LNT} := \beta \boldsymbol{D}_{LT}$.

One of the key assumptions of PIB models is that all elements within a class are assumed to have identical characteristics. For intact objects, the physical properties, such as mass and cross-sectional area, are set based on average values from the objects currently in orbit (excluding inhabited space stations). Other characteristics, like lifetime, Post-Mission Disposal (PMD) and Collision Avoidance (CA) rates are assumed based on available information. Assumed values for the considered active objects' classes are summarized in Table 1. Note that the disposal of rocket bodies is not modelled as none of the studied scenarios considers a future launch traffic for this category of objects. Hence, given that rocket bodies do not have an operational lifetime, those already in orbit are assumed to have already performed PMD manoeuvre. Lifetime, PMD rate and unavailability of CA for satellites not belonging to constellations are set based on observed trends [16][17].

*Table 1. Post-mission disposal rate, collision avoidance rate and lifetime of modelled active satellites' classes.*

| Class | PMD rate | CA rate | Lifetime [years] |
|---|---|---|---|
| Starlink | 95% | 99.9999% | 5 |
| OneWeb | 95% | 99.9999% | 10 |
| Other satellites | 40% | N/A | 8 |

A different approach is followed for defining the physical properties of the debris' classes, as mass and size data is not available for the vast majority of orbiting fragments. Space debris are modelled as spheroids with material density $\rho$ of 2,000 kg/m$^3$. Weighted averages for mass, $M$, cross-sectional area, $A_c$, and area-to-mass ratio, $A/M$, are evaluated as:

$$\begin{aligned} \overline{M}(d_1, d_2) &= \frac{\frac{\rho\pi}{6}\int_{d_1}^{d_2} w(x)\, x^3\, \mathrm{d}x}{\int_{d_1}^{d_2} w(x)\, \mathrm{d}x} \\ \overline{A_c}(d_1, d_2) &= \frac{\frac{\pi}{4}\int_{d_1}^{d_2} w(x)\, x^2\, \mathrm{d}x}{\int_{d_1}^{d_2} w(x)\, \mathrm{d}x} \\ \overline{A/M}(d_1, d_2) &= \frac{\frac{3}{2\rho}\int_{d_1}^{d_2} w(x)\, x^{-1}\, \mathrm{d}x}{\int_{d_1}^{d_2} w(x)\, \mathrm{d}x} \end{aligned} \tag{7}$$

where $w(x)$ is the weight function, which derives from Eq. (5), and can be expressed as:

$$w(d) = \frac{d^{-1.71} - d_1^{-1.71}}{d_2^{-1.71} - d_1^{-1.71}} \tag{8}$$

The three functions in Eq. (7) must be evaluated for both debris' classes, using $d_{LNT}$ and $d_{LT}$ as integration limits for the LNT debris' class, and $d_{LT}$ and $d_{\max}$ for the LT debris' class.

It is important to address a final point regarding the modelling of collision events. As mentioned earlier in this section, the object population model used in this work differentiates between catastrophic and non-catastrophic events. Consistent with standard practice [15], an energy-to-mass threshold of 40 J/g is used to determine whether an impact results in the complete destruction of the colliding objects. In other words, for any two categories of objects, $X$ and $Y$, with corresponding masses $m_X$ and $m_Y$, a collision is considered catastrophic if the following condition holds:

$$\mathrm{EMR} = \frac{1}{2}\frac{\min(m_X, m_Y)}{\max(m_X, m_Y)} v_{\mathrm{rel}}(h)^2 > 40\,\frac{\mathrm{J}}{\mathrm{g}} \tag{9}$$

with $v_{\mathrm{rel}}$ average relative velocity of impact in the shell at altitude $h$. From Eq. (9) follows that, since a single mass value is assigned to each class, impacts between objects of the classes $X$ and $Y$ at a given altitude $h$ are either all catastrophic or all non-catastrophic.

## 3 APPROACHES FOR MEASURING ORBITAL CARRYING CAPACITY

This section outlines the two primary approaches to the evaluation of OCC that the authors identified. Section 3.1 focuses on "object-based" models, with particular reference to the methodology proposed in [10]. In Section 3.2, the "risk-based" approach is examined, with an overview of various risk formulations presented in literature and considered in this study.

### 3.1 Object-based approach

Two models fall within this category. A model proposed by the Massachusetts Institute of Technology (MIT) [9] relies on determining equilibrium points for the Institute's internal source-sink debris evolutionary model, "MOCAT-3". The equilibria are reached when space activity is such that the rate at which derelict intact objects and debris are created equals their decay rate, preventing their growth in the future. Consequently, meaningful stable points can only be found in regions where atmospheric drag has a significant effect, practically limiting the analysis to altitudes below 800 km, when all possible solar activities are considered.

Sturza et al. [10] proposed an alternative formulation that, according to their analysis, guarantees general validity within the LEO region. For this reason, only this approach is considered in the comparison campaign presented in this paper. For each altitude shell, the maximum number of satellites that can be sustainably placed in orbit is the one that ensures the rate at which satellites are consumed by collisions is equal to or lower than a specified fraction $f$ of the constant rate at which satellites are launched, over a sufficiently long timeframe (e.g., 100 years). In other words, the orbital environment is propagated into the future using the source-sink model presented in Section 2, including two additional classes of objects representing a family of "probe" satellites (both active and inactive) used to test the OCC. Both state vectors are initialized to zero, and launches are performed within a single altitude shell. The deployment rate is gradually increased until the following condition is met:

$$F_P + G_P \geq f \frac{p}{\zeta_P} \tag{10}$$

where $p$ is the launch rate, and the subscript "P" indicates that the quantities refer to the probe satellites. The maximum number of satellites that can be sustainably deployed corresponds to the last launch rate value for which Eq. (10) is not satisfied. This process is applied to each altitude shell, ultimately yielding a curve that illustrates the relationship number of satellites-altitude.

### 3.2 Risk-based approach

Risk-based models rely on the use of metrics, often referred to as "space debris indices", which are formulations designed to quantify the potential threat that a space mission poses to the orbital environment. By aggregating risk values, the metrics can be extended to assess the overall threat presented by the entire population of spacecraft in orbit at any given time. When combined with long-term simulations of the orbital environment, these metrics can be used to project how the orbital health evolves over time. However, this alone is not enough to establish potential orbital capacity metrics and associated thresholds or management strategies. As highlighted in [1], a critical aspect is the identification of an acceptable and sustainable evolution of the orbital environment, which provides the foundation for applying these metrics. For example, if an agreed acceptable scenario results in an increase in the threat of a given quantity $Y$ over $X$ years, the approach would suggest that the yearly launch rate should be limited to a level that ensures the yearly increase of risk does not exceed $Y/X$.

However, it is important to note that there is no universal definition of risk, and it is unlikely that such a definition would ever exist, given the complexity and context-specific nature of the issue. The following subsections introduce the metrics used in this work. While not intended to be an exhaustive list of all indices developed in literature, the metrics have been selected to highlight the various elements of risk and their effects under different scenarios. Such elements, along with the risk principle(s) underlying each of them from the authors' perspective, are reported in Table 2.

*Table 2. Elements of risk and associated principles.*

| Element name | Meaning | Risk Principle |
|---|---|---|
| **Lifetime** | Object's natural de-orbit time | The longer an object remains in orbit, the higher the cumulative risk it poses to other objects |
| **Mass** | Object's mass | The greater the mass of an object, the more fragments it could potentially generate if it breaks up |
| **Probability** | Probability of object's breakup | The higher the probability of an object's breakup, the more likely it is to release fragments into orbit following a collision |
| **Lifetime$^2$** | Persistence in orbit of potentially released fragments | The longer the fragments generated by an object's breakup persist in orbit, the longer the exposure of other satellites to the flux associated with such fragments |
| **Congestion** | Congestion of spacecraft at the objects' altitude | The more congested the orbital environment around an object, the greater the risk the object poses to the safe operation of other spacecraft in the event of its failure and/or breakup |

The considered metrics are presented in increasing order of complexity, and for each metric, the key elements of risk it describes are identified. It is worth clarifying that, by no means, the authors intend suggesting or implying that "increasing complexity of a metric" necessarily equates to a "better metric."

### 3.2.1 Undisposed Mass Per Year

The Aerospace Corporation proposed the Undisposed Mass Per Year (UMPY) metric, which correlates the risk posed by a derelict object with its lifetime and mass. The mathematical expression for this metric reads as [18]:

$$\mathrm{UMPY} = \mathcal{F}(\mathrm{Lifetime}, \mathrm{Mass}) = \frac{1}{t_{sim}} \sum_{i=1}^{N_{in.\ obj.}} \left[ \frac{\exp\left(x \frac{t_L(h_i)}{t_{sim}}\right) - 1}{\exp(x) - 1} \right] m_i \tag{11}$$

where $N_{in.\ obj.}$ is the total number of inactive objects; $t_{sim}$ is the time period over which the orbital environment is propagated; $t_L$ is the object's lifetime computed from an orbit altitude $h_i$, and $m_i$ its mass; $x$ is the lifetime scaling exponent, which is set to 4 as in [18].

### 3.2.2 Criticality of Spacecraft Index

The Criticality of Spacecraft Index (CSI), proposed by Rossi et al. [19], introduces a dependency on the probability that the derelict object may fragment under the effect of an in-orbit collision. Such Probability of Collision (PoC) does not practically appear in the formulation, but rather a simple dependency on the spatial density, $n_r$, at the object altitude (upon which the PoC depends) is included. The metric equation is as follows [19]:

$$\mathrm{CSI} = \mathcal{F}(\mathrm{Lifetime}, \mathrm{Mass}, \mathrm{Probability}) = \sum_{i=1}^{N_{in.\ obj.}} m_i\, t_L(h_i)\, n_r(h_i) \tag{12}$$

Note that, in the original formulation, each of the terms in the equation is scaled by a reference value to obtain a non-dimensional formulation. Such terms are here omitted, as any result shown in Section 6 is presented in relative terms with respect to a reference scenario.

### 3.2.3 Fragment-Years

The Fragment-Years (FRY) index, that the European Space Agency proposed in [1], introduces the squared dependency on the lifetime, by including in the formulation the integral of a function $P(t,h)$, which describes the percentage of the fragments larger than 10 cm still in orbit after a given time $t$ following the object's breakup. The function $P(t,h)$ is obtained by least square fitting of the results on decay time of fragmentation clouds simulated with the NASA SBM. The FRY index takes the form:

$$\mathrm{FRY} = \mathcal{F}(\mathrm{Lifetime}^2, \mathrm{Mass}, \mathrm{Probability}) = \sum_{i=1}^{N_{obj.}} F_{c,cat}(h_i)\, A_{c_i}\, t_L(h_i)\, 5.13 m_i^{0.75} \times \int_0^{t_s} P(t,h_i)\, \mathrm{d}t \tag{13}$$

with $N_{obj.}$ number of intact objects, $F_{c,cat}$ flux of objects capable to trigger the catastrophic collision of the object, and $A_{c_i}$ object's average cross-sectional area. The exponent of the mass, 0.75, and the multiplicative factor, 5.13, result from the number of fragments generated by a collision as predicted by the NASA SBM [15] - *see* Eq. (5). The multiplicative factor is obtained when setting the minimum characteristic length $L_c$ to 10 cm.

### 3.2.4 University of Strathclyde Index

The index proposed by Wilson et al. [20] of the University of Strathclyde, here referred to as IDX-STR, while keeping the already introduced key elements of risk, includes the dependency on the congestion of satellites at the altitude of the probe object, in the attempt to measure the incremental risk that its potential breakup would cause on other orbiting spacecraft. With respect to the original formulation of the index proposed in [20], a different approach is here used for evaluating the probability of collision, in order to keep consistency on how this aspect is modelled across the considered metrics. Indeed, the original paper uses a methodology based on the Minimum Orbital Intersection Distance (MOID), while this work adopts a flux-based approach. Therefore, in this paper, the index has the following mathematical expression:

$$\mathrm{IDX-STR} = \mathcal{F}(\mathrm{Lifetime}^2, \mathrm{Mass}, \mathrm{Probability}, \mathrm{Congestion}) = \sum_{i=1}^{N_{obj.}} F_{c,cat}\, A_{c_i}\, t_L(h_i)\, a\, m_i^{0.75} n_r(h_i)^b t_{decay}(h_i) \tag{14}$$

where the last term is the decay time function for fragmentation clouds generated at the altitude of the object $h_i$, and $a$ and $b$ are factors, which the authors set to $2.31 \times 10^4$ and 0.229, respectively, to model objects orbiting within the LEO region.

### 3.2.5 THEMIS Index

The THEMIS index [21][22], developed within the homonymous ESA's project carried out by Politecnico di Milano in collaboration with DEIMOS UK, treats the congestion term in a more elaborated form. The effect of the potential fragmentation of the object is measured as incremental collision probability for the active satellites with which the orbit of the ejected fragments can intersect. Hence, this index provides a direct measure of the consequences of a breakup as potential loss for spacecraft operators. The THEMIS index takes the following form:

$$\begin{aligned}&\text{THEMIS}\\&=\mathcal{F}(\text{Lifetime}^2,\text{Mass},\text{Probability},\text{Congestion})\\&=\sum_{i=1}^{N_{obj.}} F_{c,cat}\,(h_i)A_{c_i}\,t_L(h_i)\sum_{j=1}^{N_{act.obj.}} P_{c,ind.ij}(t_p)\end{aligned} \tag{15}$$

where $N_{act.obj.}$ is the number of active objects, and $P_{c,ind.ij}$ is the PoC induced by the fragmentation cloud associated to the breakup of the i$^{th}$ object on the j$^{th}$ active satellite.

Since IDX-STR and THEMIS evaluate the consequences of a potential fragmentation of an object on other spacecraft, they offer flexible analysis depending on the desired focus. For example, let us consider the case of evaluating the impact of a satellite constellation. If the purpose of the analysis consists in determining the effect on "neighbouring" operators, the analysis would focus solely on measuring the impact of potential fragmentation of the constellation's satellites on the other orbiting satellites, excluding the constellation's own satellites. The operator of the constellation, on the other hand, may be more concerned with assessing the consequences of imperfect management on its business case. In this case, only the risk to its own satellites, referred to as the "self-effect," would be calculated. Finally, if evaluating the consequences on the orbital environment, particularly in terms of increased debris pollution, the combined effect would be analysed. Section 4 will provide results from analyses that include or exclude such self-effect.

# 4 COMPARING ORBITAL CARRYING CAPACITY MODELS

This section focuses on the OCC models introduced in Section 3. First, it evaluates the maximum number of satellites that can be placed sustainably within defined altitude shells, following the object-based approach outlined in Section 3.1. Next, it provides a detailed analysis of the various risk metrics presented in Section 3.2, examining how the deployment of satellite constellations at different altitudes is assessed by the considered risk formulations and evaluating how variations in constellation characteristics and control parameters influence the perceived risk. Finally, it compares the two primary approaches to OCC measurement identified by the authors.

## 4.1 Object-based approach: Satellite-altitude curve

The object-based approach discussed in [10] and introduced in Section 3.1 is used to derive the curve representing the maximum number of satellites that can be sustainably placed in orbit as a function of altitude. It is important to note that this curve is not uniquely defined. In fact, it inherently depends on the specific characteristics of the probe satellites being considered, including their size, mass, operational lifetime, PMD success rate, and collision avoidance capabilities. The results presented in the following sections are based on the arbitrary characteristics specified in Table 3.

*Table 3. Characteristics of the modelled probe satellites to test OCC models.*

| **Quantity** | **Value** |
|---|---|
| Cross-sectional area [m$^2$] | 10 |
| Mass [kg] | 500 |
| Lifetime [years] | 10 |
| PMD rate | 95% |
| CA rate | 99.9999% |

Additionally, the satellites-altitude curve is influenced by the accepted level of risk, which in the formulation presented in [10] is represented by the parameter $f$. This parameter denotes the accepted fraction of launched satellites that may be lost due to collisions over their lifetime. This condition must hold at any point in time throughout the considered timeframe, during which the in-orbit population is propagated. In this study, the propagation period is set to 100 years and the fraction $f$ to 1%. In general, different assumptions on these two parameters are likely to lead to results different than what illustrated below.

Figure 1 illustrates the satellite-altitude curve within the altitude range of 200-1600 km. According to the considered settings, the object-based approach predicts that an effectively infinite number of satellites can be placed below 450 km. Beyond this, an exponential decrease occurs in the altitude range of [450, 680) km, which drives the curve to zero in the highly congested region between 680 and 950 km. At higher altitudes, the curve shows an initial exponential increase in the range of [950, 1100) km, followed by a plateau in the high-LEO region. This plateau is primarily due to the combined effects of negligible atmospheric drag at these altitudes and the very low levels of satellite and debris traffic.

The results illustrated in Figure 1 will be used in Section 4.3 to compare the object-based approach with the risk-based approach.

## 4.2 Risk-based approach: Impact of constellations deployment

The risk metrics presented in Section 3.2 are applied here to evaluate the risk increase across different scenarios in terms of satellite launch traffic. Specifically, this study seeks to determine how different risk formulations quantify the impact on the orbital environment resulting from the deployment of satellite constellations in LEO at

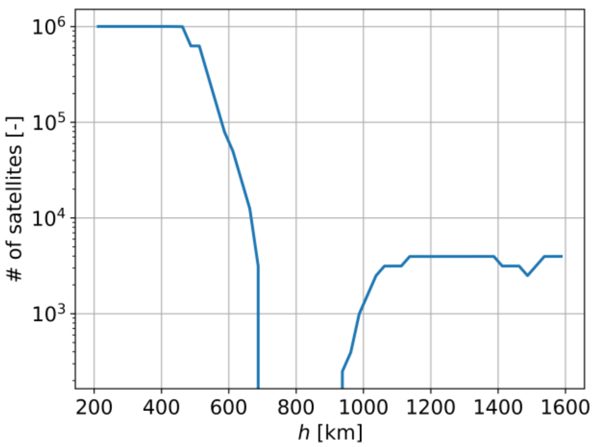


*Figure 1. Maximum number of satellites that can be sustainably placed in orbit as a function of altitude according to the formulation in [8].*

different altitudes (Section 4.2.1) and the sensitivity of these formulations to variations in constellation characteristics (Section 4.2.2). This will help in evaluating the suitability of these metrics for assessing the space sustainability of missions, depending on the characteristics of their orbits. It is important to note that this analysis aligns with the approach proposed in Section 4.1, that considers the deployment of probe satellites with identical characteristics at the same altitude, which can be thought of as composing a unique constellation. This parallelism facilitates a comparison of the two approaches, as discussed in Section 4.3.

#### 4.2.1 Influence of deployment altitude on measured risk

The cases analysed involve the deployment of satellite constellations at altitudes of 650 km and 1300 km. Although both constellations are in LEO, these scenarios differ significantly. At 650 km, atmospheric drag has a considerable impact on the orbital evolution of objects, offering a significant advantage from a space sustainability perspective, because satellites that fail at this altitude will re-enter the atmosphere after a certain time even if not subject to any manoeuvre. In contrast, at altitudes above 1000 km, the atmosphere is too thin to cause substantial orbital decay. However, low-altitude orbits are far more congested, meaning that poor space system management can lead to operational physical interference with neighbouring satellites. Therefore, understanding how the deployment of the two system is perceived by the various risk metrics and, thus, how these key differences in risk are captured by them, is essential for their appropriate application. This is the ultimate goal of this section.

The risk metrics are compared based on the measured risk increment associated with the deployment of the two constellations relative to a baseline scenario. This baseline, referred to as Business-As-Usual (BAU), assumes a launch traffic that maintains the number of currently in-orbit active satellites constant over time. The risk increment is evaluated according to the following steps:

1. The orbital environment is propagated under the BAU scenario.
2. The orbital environment is also propagated by incorporating the deployment of the two satellite constellations mentioned above into the BAU launch traffic, each of them modelled in a separate simulation. These two scenarios, referred to as Low-Altitude Constellation Deployment (LACD) and High-Altitude Constellation Deployment (HACD), respectively, assume that both systems are deployed and continuously replenished to maintain a constant number of active satellites in orbit.
3. The aggregate risk, defined as the sum of the risk of all objects in orbit, is computed for the three simulation scenarios at multiple times over the considered 100-year timeframe.
4. The percentage risk increment, $\delta R_{\%}$, due to the constellation deployment is calculated at any given time $t$ according to the following expression:

$$\delta R_{\%}(t) = \frac{R(t) - R_{\mathrm{BAU}}(t)}{R_{\mathrm{BAU}}(t)} \cdot 100 \qquad (16)$$

where $R_{\mathrm{BAU}}$ and $R$ are the aggregate risk for the BAU case and for either LACD or HACD cases, respectively, evaluated using each risk metric.

For the nominal case, the same characteristics listed in Table 3 are applied to the satellites of both constellations, with the constellation size assumed to be as large as 1,000 satellites. These parameters will be subsequently varied in Section 4.2.2 to test the sensitivity of the metrics to their variations.

The dot chart in Figure 2, used to present all the results throughout this section, shows the maximum percentage risk increment over the simulation period, as measured by each of the risk metrics. It also includes other quantities derived directly from the simulations of the orbital environment. In particular, the chart reports the increase in both LT and LNT debris, as well as in the catastrophic and non-catastrophic collision rates.

The first key observation is that the quantified risk increment varies significantly across the different metrics in both scenarios. Analysing each measured quantity in more details, it can be noted that HACD results in a larger population of in-orbit debris, primarily due to the absence of atmospheric drag and, hence, of a significant sink mechanism. However, this increased debris population does not lead to a notably higher threat in terms of collision events. While the rate of catastrophic collisions is slightly higher, the rate of non-catastrophic ones is significantly lower. The HACD "performs" worse when assessed using metrics that relate risk to the persistence of uncontrolled spacecraft in orbit, such as CSI and UMPY. Conversely, the LACD "performs" worse when evaluated with metrics that focus on the risk posed to other satellites, such as IDX-STR and THEMIS when excluding self-effects. When the self-effect is included, similar risk values are observed, with the self-effect being more significant at higher altitudes. Interestingly, the FRY metric, which "bridges" formulations based on the persistence of derelict objects in orbit and those focused on secondary effects like induced collisions, estimates a similar risk increment for the two scenarios.

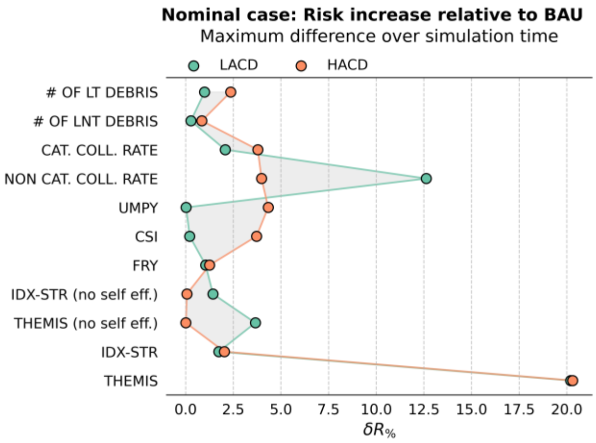


*Figure 2. Risk increment relative to BAU due to constellations deployment at different altitudes.*

Another important aspect to consider is how the risk increment evolves over time. In fact, it is crucial to recognize that when conducting long-term analyses (e.g., over 100 years), accurately predicting the future evolution of the space environment is extremely challenging and likely unattainable, given the unpredictable nature of launch traffic and technological advancement, with the latter inevitably influencing satellite design and operation (e.g., de-orbiting services may significantly reduce the burden associated with satellites failures and new design features may make spacecraft less likely to fragment following the impact with a space debris). In other words, the longer the propagation time, the larger the uncertainty in the results. Additionally, from the perspective of operators potentially affected by the constellation deployment, the evaluation of its effects in the shorter term would likely be deemed of greater interest. In this regard, Figure 3 illustrates the difference in the percentage risk increment relative to BAU between the two constellation deployment scenarios. In mathematical terms, the figure displays how the metrics assess the following quantity:

$$\Delta[\mathrm{H}-\mathrm{L}]_{\%} = \delta R_{\%}^{\mathrm{HACD}} - \delta R_{\%}^{\mathrm{LACD}} \qquad (17)$$

with $\delta R_{\%}^{\mathrm{HACD}}$ and $\delta R_{\%}^{\mathrm{LACD}}$ risk increment relative to BAU for HACD and LACD scenarios, respectively. Since the focus is on the difference in risk increase, a null value indicates that both scenarios pose the same level of threat. Generally, during the first half of the simulation, the LACD results in a higher environmental threat as measured by the majority of the metrics (negative $\Delta[\mathrm{H}-\mathrm{L}]_{\%}$ values), with the data points shifting to the right (towards less negative or positive $\Delta[\mathrm{H}-\mathrm{L}]_{\%}$ values) over time. This outcome is expected: since the high-altitude region is less congested, it takes time for satellite failures due to unsuccessful post-mission disposal to accumulate, interact with each other and with the background debris population before leading to an observable threat. In other words, over time, the lack of atmospheric drag at 1300 km altitude leads to the accumulation of derelict spacecraft, causing the risk to gradually increase. In contrast, at low altitudes, the impact of the new system is immediately perceived. However, the risk increment over time is less pronounced because atmospheric drag plays a more significant role in mitigating risk.

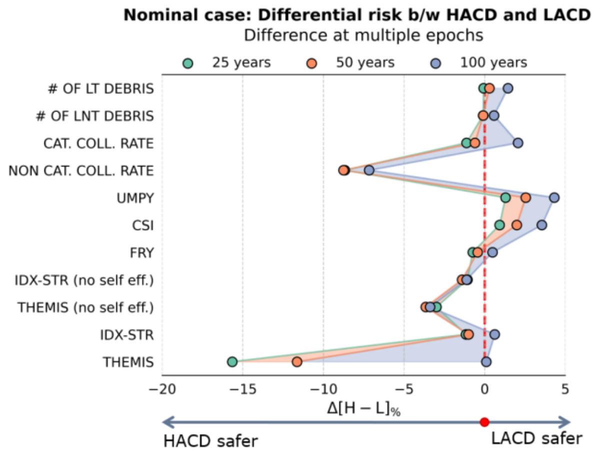


*Figure 3. Difference in risk increment relative to BAU between LACD and HACD scenarios at multiple epochs.*

### 4.2.2 Sensitivity of metrics to constellation characteristics

This section explores how variations in the characteristics of the constellations, from size to the effectiveness of mitigation measures, and the deployment of constellations in adjacent shells, impact the perceived risk as assessed by the considered risk metrics. Specifically, the dot charts that are presented below investigate how these variations shift the balance in differential risk between HACD and LACD. Therefore, within this section the quantity under analysis (i.e., the x-axis of the dot charts), indicated with $\varepsilon$, takes the following form:

$$\varepsilon = \Delta[\mathrm{H}-\mathrm{L}]_{\%}^{\mathrm{mod.}} - \Delta[\mathrm{H}-\mathrm{L}]_{\%}^{\mathrm{nom.}} \qquad (18)$$

where $\Delta[\mathrm{H}-\mathrm{L}]_{\%}^{\mathrm{mod.}}$ and $\Delta[\mathrm{H}-\mathrm{L}]_{\%}^{\mathrm{nom.}}$ are the differential risks between HACD and LACD considering the nominal (Table 3) and modified constellation characteristics, respectively. The following considerations can be made regarding the variable $\varepsilon$:

- If $\varepsilon \approx 0$, the analysed change in constellation characteristics does not affect the balance of differential risk between HACD and LACD scenarios. In other words, the relative risk remains the same as shown in Figure 3.
- If $\varepsilon < 0$ ($\varepsilon > 0$), the analysed change in constellation characteristics has a greater negative impact (i.e., a relative increase in risk) on the safety associated with the constellation at low (high) altitude. Naturally, the greater the difference, in absolute value, the higher the relative impact.

**Sensitivity to mitigation action**

First, the impact of variations in the post-mission disposal success rate and the effectiveness of collision avoidance manoeuvres is analysed. Figure 4 illustrates how the differential risk between HACD and LACD changes as the PMD rate decreases from 95% to 90%. With the exception of the two metrics that focus on the negative impact on neighbouring operators (i.e., IDX STR and THEMIS excluding self-effect), a reduction in de-orbiting reliability has a more significant impact on constellations at high altitudes. Naturally, the larger number of uncontrolled satellites remaining in orbit where atmospheric drag is negligible causes metrics like UMPY and CSI, which directly correlate risk to the number of abandoned spacecrafts, to increase linearly. The significant change in the value assessed by THEMIS, particularly the large difference compared to the case when self-effect is excluded, highlights that the most substantial negative impact is on the constellation satellites themselves. As noted previously, HACD accumulates risk in a non-linear fashion over time, with a shift towards long-term consequences.

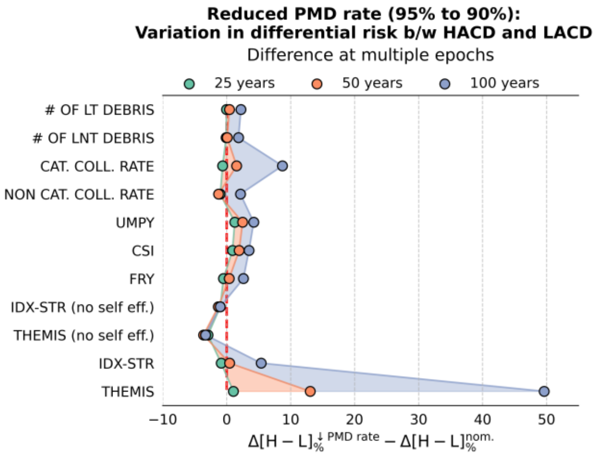


*Figure 4. Effect of reduced post-mission disposal rate on the differential risk between HACD and LACD scenarios.*

Similarly, Figure 5 displays the effect of reducing the CA rate from 99.9999% to 99.99%. It is important to note that this reduction is considerably smaller than the one considered in the PMD analysis. The values used in the study are intended to represent realistic scenarios: an accepted risk threshold in the case of conjunction of more than 1:10,000 would be outside the current standards in practice. Less stringent CA measures have a greater negative impact on the constellation at low altitude, particularly in terms of increased risk for nearby operators. Instead, the small change in CA rate is not sufficient to cause a relevant increase in the number of failures; in fact, the balance between HACD and LACD scenarios is unchanged as monitored by UMPY and CSI metrics.

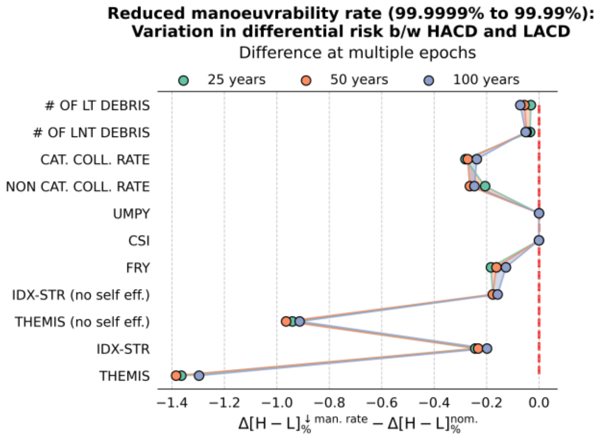


*Figure 5. Effect of reduced collision avoidance rate on the differential risk between HACD and LACD scenarios.*

**Sensitivity to constellation and satellite size**

The effect of increasing the number of satellites in the two constellations, from 1,000 to 2,000 satellites, and the size of the satellites, from 500 kg to 1,000 kg, is shown in Figure 6 and Figure 7. In the latter case, the cross-sectional area is doubled accordingly to maintain the same area-to-mass ratio. It is important to note that the two analysed cases are closely related. Doubling the number of satellites results in the same increase in collision rate as doubling the satellite cross-sectional area, as the cumulative constellation cross-sectional area coincides. However, the increase in size also leads to a higher number of released fragments in the event of a collision. Nevertheless, similar trends are observed, and the same considerations can be drawn for both analyses.

The considered changes have a slightly greater effect on the HACD in terms of the number of both LT and LNT debris. Interestingly, an opposite effect is observed for catastrophic and non-catastrophic collisions: the number of catastrophic collisions increases more for the HACD case, while the number of non-catastrophic collisions increase more for the LACD case. Considerations analogous to those highlighted for the PMD rate analysis can be made for the metrics, with the increase in self-effect driving the notable shift to the right (i.e., penalizing HACD) in the THEMIS estimates over the long term. However, within the first 25 years, the trend is reversed, demonstrating how the increase in constellation and satellite sizes takes time to negatively impact on the accumulation of failed satellites and debris at higher altitudes.

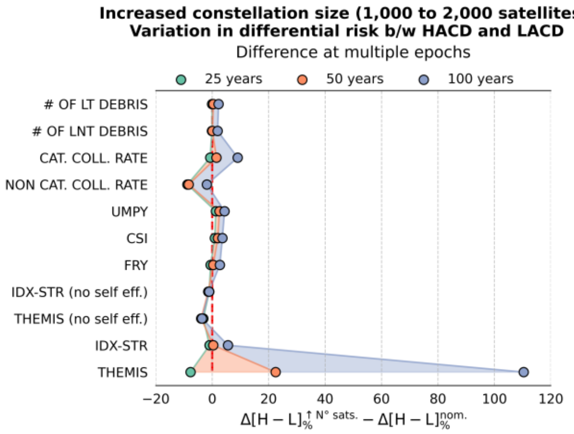


*Figure 6. Effect of increased constellation size on the differential risk between HACD and LACD scenarios.*

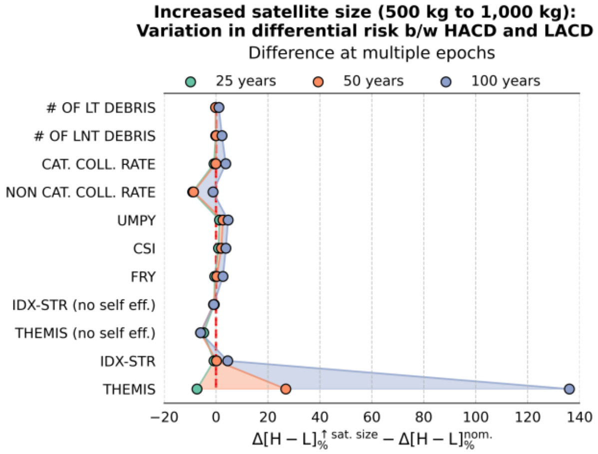


*Figure 7. Effect of increased satellite size on the differential risk between HACD and LACD scenarios.*

**Sensitivity to constellation proximity**

Lastly, the effect of deploying two constellations in close proximity (i.e., in adjacent shells) is investigated. The analysis explores how the balance between HACD and LACD may vary due to the two systems potentially influencing negatively each other (e.g., the failure of one system possibly impacting the other), which could ultimately lead to a higher threat for neighbouring operators. The two additional constellations, with the same characteristics as those considered in the nominal case and listed in Table 3, are deployed in the two nearest adjacent shells at lower altitude, at 625 km and 1,275 km, respectively. The resulting dot chart is represented in Figure 8. Operating the two constellations in close proximity at low altitude hugely impact the neighbouring active satellites, as measured by the THEMIS formulation without self-effect. As for the other metrics, UMPY and CSI estimates are consistently in the positive side of the chart, while for IDX-STR and THEMIS with self-effect the already commented rightward trend as time passes is observed.

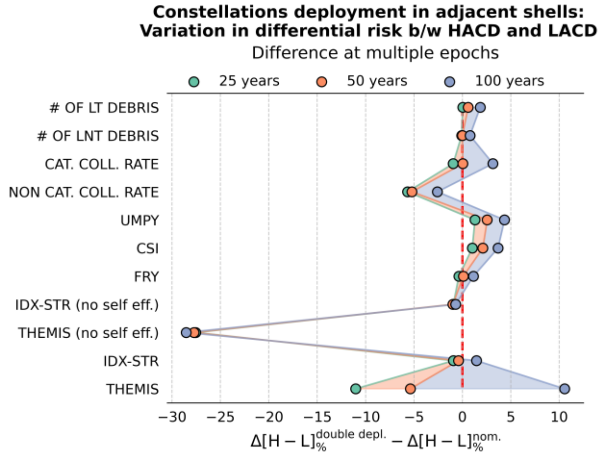


*Figure 8. Effect of the deployment of constellations in adjacent shells on the differential risk between HACD and LACD scenarios.*

It is worth noting that the FRY metric exhibits the least variation in the balance between HACD and LACD scenarios, regardless of the applied modification compared to the nominal case. This further demonstrates its intermediary role, with results positioned between formulations focused on the persistence of derelict objects in orbit and those focused on secondary effects like caused collisions.

To interpret graphically the sensitivity of the analysed risk metrics to variations in constellation characteristics, depending on the constellation altitude, spider charts are generated following these steps:

1. The maximum risk increment over the simulation time (i.e., 100 years) resulting from variations in constellation characteristics is computed for both the LACD, $\delta R_{\mathrm{LACD}}$, and HACD, $\delta R_{\mathrm{HACD}}$, cases for each metric.
2. For each studied constellation's change in characteristics, the maximum risk increment, $\delta R_{\max}$, measured by the considered metrics, is identified.
3. The sensitivity of each metric is then computed as:

$$s = \log_{10}\left(\frac{\delta R_{\mathrm{LACD/HACD}}}{\delta R_{\max}}\right) \qquad (19)$$

Note that $\delta R_{\max}$ is the overall maximum risk increment among all metrics, for both the LACD and HACD scenarios, associated with a change in one of the constellation characteristics.

The resulting spider charts related to the LACD and HACD scenarios are shown in Figure 9. Note that each level change in the graph (i.e., moving outward by one circle) corresponds to an order of magnitude change in risk, due to the logarithmic scale.

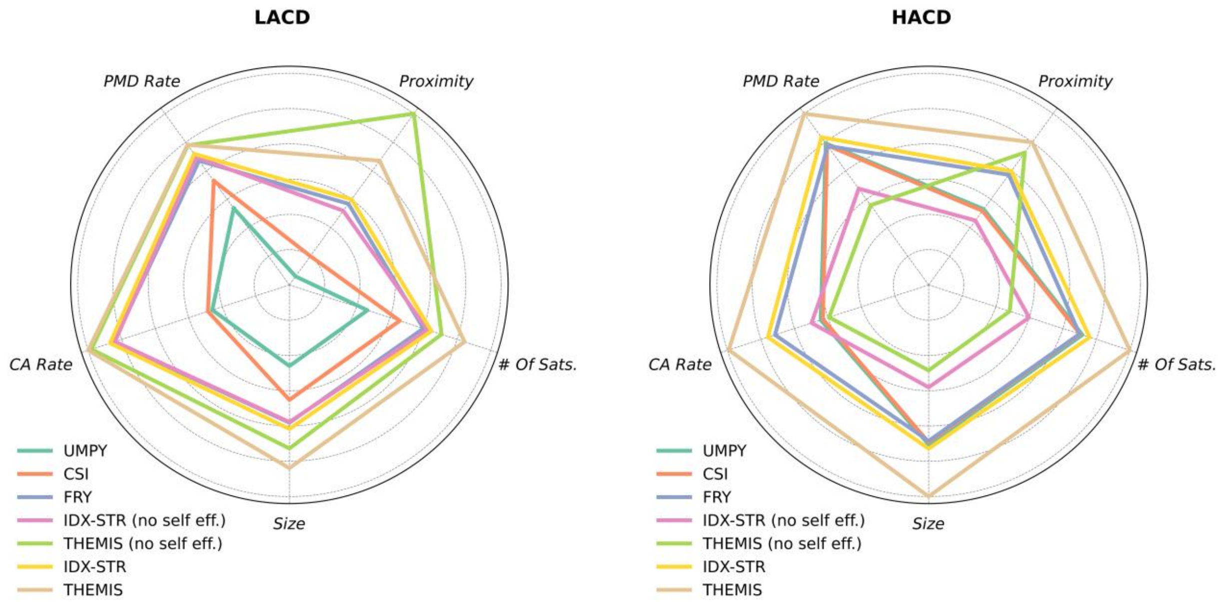


*Figure 9. Metrics sensitivity to variations in constellation characteristics for LACD (left) and HACD (right) scenarios.*

Although no new content is added compared to the previous analyses in this section, the two spider charts provide direct insights into how the metrics differently perceive the risk associated with the deployment of the two constellations. Specifically, the perceived risk, as measured by the UMPY and CSI metrics, is more influenced by changes in constellation characteristics in the HACD case than in the LACD case. Although in different magnitude, these two metrics are highly sensitive to variations in PMD rate, constellation and satellite sizes in both deployment scenarios, as such changes have direct impact on the number of derelict objects in orbit. In contrast, the IDX-STR and THEMIS metrics show an opposite trend when excluding self-effect, as they attribute a greater impact to the LACD case. Moreover, they are very sensitive to CA rate and constellation proximity, as these changes affect the physical interference of the deployed systems with neighbouring satellites. When self-effect is accounted for, THEMIS demonstrates the highest sensitivity to changes in characteristics in both scenarios, though the underlying causes differ: at low altitude, sensitivity is strongly linked to the incremental threat to neighbouring satellites, whereas at high altitude, the threat is mainly perceived by the constellation itself. As noted earlier, the FRY metric exhibits the most similar behaviour in both scenarios.

## 4.3 Object-based vs Risk-based approach

To compare the object-based and risk-based approaches, the satellite-altitude curve from Section 4.1 is used as an input to the risk analysis, following the methodology outlined in Section 4.2. Specifically, for each altitude shell, the maximum number of satellites that can be placed sustainably in orbit according to the object-based approach is treated as a constellation deployment scenario. For each scenario, the associated risk increments, as determined by the risk formulations, are calculated. Note that each constellation deployment is treated as a separate simulation, with its own long-term environmental propagation and risk increase evaluation relative to the BAU scenario. The outcome of this analysis is a series of risk-altitude curves, one for each metric. These curves illustrate the estimated risk increment by each metric as a function of altitude, resulting from the deployment of constellations with sizes shown in Figure 10. If a metric predicts a flat risk-altitude profile, with exception of the altitude range [680, 950) km where no satellites are deployed, it indicates that the same risk increment is associated with the deployment of the constellations of varying sizes, suggesting that the metric perceives risk in the same way as the object-based approach. In contrast, significant differences in risk increment must be interpreted as a strong disagreement between the metric and the object-based approach. The resulting charts are presented in Figure 10 for various simulation times, consistently with previous analyses.

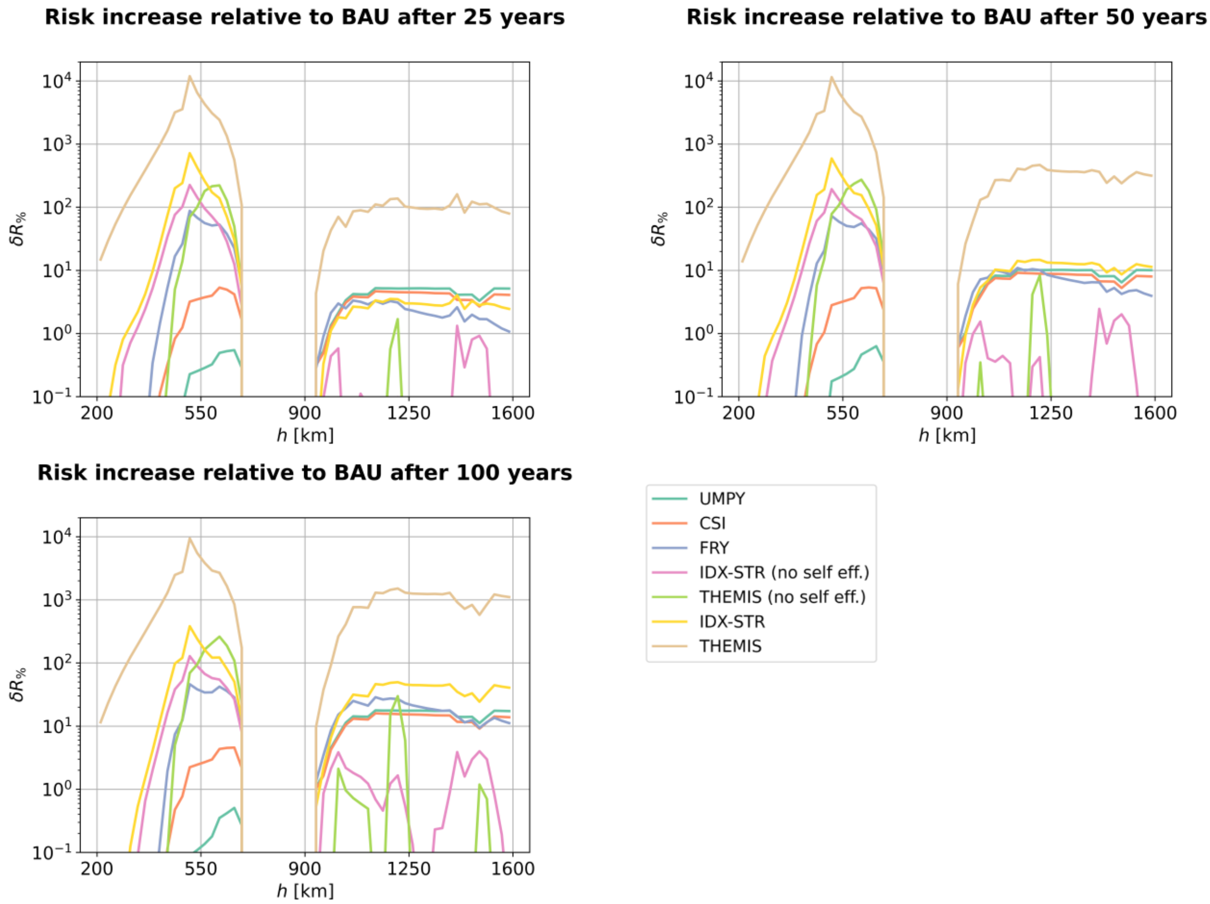


*Figure 10. Risk increment due to constellations deployment relative to BAU, with constellation size varying based on altitude and according to the satellite-altitude curve from the object-based approach.*

As already mentioned in Section 4.2, the risk increment remains approximately constant over time at low altitudes, whereas at higher altitudes, a non-linear dependency of risk on time is observed. Interestingly, some metrics clearly detect the presence of already deployed constellations, a feature that was not fully captured in the satellite-altitude curve. Specifically, THEMIS, IDX-STR, and FRY exhibit a significant peak just below 550 km (the altitude of the Starlink constellation), while IDX-STR and THEMIS, excluding self-effects, show sharp spikes around 1200 km (the altitude of the OneWeb constellation). UMPY is the only metric that estimates a higher threat at high altitudes, regardless of simulation time. Among the formulations studied, CSI shows the highest agreement with the object-based solution, displaying the most similar risk increment values below 680 km and above 950 km, excluding very low altitudes. This suggests that the object-based model primarily captures the risk associated with the permanence of derelict objects in orbit and their collision probability. The remaining metrics estimate a significantly higher threat at low altitudes, which slightly diminishes over time. Therefore, it is reasonable to conclude that the object-based approach tends to underestimate the risk posed by constellation deployment at low altitudes, at least when compared to the risk-based formulations analysed in this paper.

## 5 CONCLUSIONS

This paper presented the software architecture developed by Telesat to compare existing Orbital Carrying Capacity (OCC) models. Specifically, it examined the two primary OCC approaches identified by the authors, analysing them both theoretically and through practical test cases. The first approach proposes a methodology to determine the maximum number of satellites that could be sustainably placed within defined altitude shells, based on an accepted risk threshold that limits the fraction of satellites lost to collisions over a sufficiently long-time horizon. The second correlates the residual availability of orbital resources with the cumulative risk posed by the current and projected spacecraft populations under an acceptable evolution of the orbital environment. This second approach ramifies into multiple formulations that consider a different definition of risk associated with a space mission. This study focused on evaluating how the deployment of constellations at varying altitudes expends such orbital resources, as predicted by different OCC models.

A substantial part of the analysis was dedicated to comparing various risk metrics that have been proposed over the years, some of which remain under development. The findings demonstrated that the same satellite launch traffic scenario can be evaluated in markedly different ways depending on the selected metric. This underscores the fact that an arbitrary choice of methodology may yield only a partial assessment of the actual risks associated with a studied future launch activity. From Telesat's perspective, no current single metric can be considered universally applicable, as every metric highlights different key aspects of risk. For instance, the deployment of a constellation at high altitude presents a greater risk in terms of the prolonged persistence of failed satellites in orbit compared to the same deployment at low altitude. However, this risk does not directly translate into an immediate hazard for other operators, but it rather results in the gradual accumulation of debris, which could ultimately impact the constellation itself, in the absence of remediation measures. Conversely, the unsuccessful de-orbiting of constellation satellites or the imperfect execution of collision avoidance manoeuvres at lower altitudes leads to an immediate increase in risk for neighbouring satellites or other large systems in adjacent orbital shells. Nevertheless, given the current standard practices employed by large operators, it is unlikely that this induced risk causes a significant long-term escalation in orbital debris within lower altitude shells, given the efficient sink mechanism provided by atmospheric drag. Every space system entails potential risks, but accurately characterizing them may require distinct considerations and methodologies. This flexible approach ensures that any resulting Orbital Carrying Capacity framework effectively protects the long-term sustainability of the orbital environment, while adequately considering the diverse nature of space systems.

## 6 REFERENCES


1. Krag, H., Lemmens, S. & Letizia, F. (2017). Space traffic management through the control of the space environment's capacity. *1$^{st}$ IAA Conference on Space Situational Awareness*, Orlando, Florida, USA.

2. McKnight, D., Witner, R., Letizia, F., et al. (2021). Identifying the 50 statistically-most-concerning derelict objects in LEO. *Acta Astronautica* 181, 282-291.

3. Letizia, F., Colombo, C., Rossi, A., et al. (2024). Mission-based and environment-based approaches for assessing the severity of a space debris evolution scenario from a sustainability perspective. *75$^{th}$ International Astronautical Congress*, Milan, Italy.

4. McKnight, D., Dale, E., Colombo, C., et al. (2024). Normalizing Orbital Capacity Characterization. *75$^{th}$ International Astronautical Congress*, Milan, Italy.

5. Lifson, M., Giudici, L., Neri, M., et al. (2025). A "Menu" of kinetic space safety metrics to support space environment objectives. *11$^{th}$ Space Traffic Management Conference,* Austin, Texas, USA.

6. Talent, D. L. (1992). Analytic model for orbital debris environmental management. *Journal of Spacecraft and Rockets* 29(4), 508–513.

7. Rossi, A., Cordelli, A., Farinella, P., Anselmo, L., & Pardini, C. (1997). Long term evolution of the space debris population. *Advances in Space Research* 19(2), 331–340.

8. Somma, G. (2019). Adaptive remediation of the space debris environment using feedback control. PhD thesis, University of Southampton.

9. Jang, D., D'Ambrosio, A., Lifson, M., Pasiecznik, C., & Linares, R. (2022). Stability of the LEO Environment as a Dynamical System. *The Advanced Maui Optical and Space Surveillance Technologies (AMOS) Conference*, Maui, Hawaii, USA.

10. Sturza, M.A., Dankberg, M.D & Blount W.N. (2022). LEO Capacity Modeling for Sustainable Design. *The Advanced Maui Optical and Space Surveillance Technologies (AMOS) Conference,* Maui, Hawaii, USA.

11. Liou, J.-C. (2004). LEGEND - a three-dimensional LEO-to-GEO debris evolutionary model. *Advances in Space Research* 34(5), 981–986.

12. Bastida Virgili, B. (2016). DELTA debris environment long-term analysis. *International Conference on Astrodynamics Tools and Techniques*, Darmstadt, Germany.

13. U.S. Air Force, https://www.space-track.org/ (accessed 03.03.2025).

14. European Space Agency, https://discosweb.esoc.esa.int/ (accessed 03.03.2025).

15. Johnson, N.L., Krisko, P.H., Liou, J.-C. & Anz-Meador, P.D. (2001). NASA's new breakup model of evolve 4.0. *Advances in Space Research* 28, 1377-1384.

16. ESA Space Debris Office, ESA's Annual Space Environment Report, 2024.

17. Letizia, F., Bastida Virgili, B. & Lemmens, S. (2023). Assessment of orbital capacity thresholds through long-term simulations of the debris environment. *Advances in Space Research* 72(7).

18. Henning, G.A., Sorge, M.E., Bologna, D.G., et al. (2024). Correlating LEO Sustainability to Targeted Debris Mitigation Methods Using a Simple Metric. *75$^{th}$ International Astronautical Congress*, Milan, Italy.

19. Rossi, A., Valsecchi, G.B. & Alessi, E.M. (2015). The Criticality of Spacecraft Index. *Advances in Space Research* 56, 449-460.

20. Wilson, C., Vasile, M., Feng, J., et al. (2024). Extending a Risk Metric for Individual Missions to Evaluate Overall Risk in Orbit. *75th International Astronautical Congress*, Milan, Italy.

21. Letizia, F., Colombo, C., Lewis, H. & Krag, H. (2017). Extending the ECOB space debris index with fragmentation risk estimation. *7th European Conference on Space Debris*, Darmstadt, Germany.

22. Colombo, C., Giudici, L., Muciaccia, A., et al. (2023). Assessment of the collision risk in orbital slots and the overall space capacity. *2nd International Orbital Debris Conference*, Houston, Texas, USA.